Title**: The 2015 Eruption of Axial Seamount: Seismic Constraints on Caldera Dynamics**

One Sentence Summary:
An outward dipping ring fault zone beneath a submarine caldera accommodates inflation and guides a seafloor eruption.

Authors:
William S. D. Wilcock[1], Maya Tolstoy[2], Felix Waldhauser[2], Charles Garcia[1], Yen Joe Tan[1], Delwayne R. Bohnenstiehl[3], Jacqueline Caplan-Auerback[4], Robert P. Dziak[5], Adrien F. Arnulf[6] and Michael Mann[3]

Affiliations:
1 – School of Oceanography, University of Washington, Seattle WA 98195
2 – Lamont-Doherty Earth Observatory, Columbia University, Palisades, NY 10964
3 - Department of Marine, Earth and Atmospheric Sciences, North Carolina State University, Rayleigh, North Carolina 27695
4 - Geology Department, Western Washington University, Bellingham, WA 98225.
5 - National Oceanic and Atmospheric Administration (NOAA), Pacific Marine Environmental Laboratory, Newport, OR 97365
6 - Institute for Geophysics, Jackson School of Geosciences, University of Texas, Austin, Texas 78758

Abstract:
Seismic observations in volcanically active calderas are challenging and as such the understanding of their internal dynamics is limited. A recently installed observatory atop Axial Seamount on the Juan de Fuca ridge allows unprecedented real-time monitoring of a submarine caldera. Beginning on April 24th 2015, the seismic network captured an eruption that culminated in explosive acoustic signals at sites where lava erupted on the seafloor. Extensive seismic activity preceding the eruption shows that inflation is accommodated by the re-activation of an outward dipping caldera ring fault, with strong tidal triggering indicating a critically stressed system. The geometry of the ring fault puts the caldera into compression as the volcano inflates and guides the dike along the side of the caldera before it steps into a volcanic rift.

Main Text:
On land, seismic monitoring is one of the most widely used tools for characterizing volcanic cycles (Zobin, 2013). Submarine volcanoes account for 80-90% of the Earth's volcanism (Crisp, 1984) but it has proved difficult to observe their eruptions with autonomous local seismic networks because of the challenges of sustaining long-term observations and recovering instruments after an eruption (Tolstoy et al., 2006). However, the volcanoes that form mid ocean ridges have several characteristics that make them ideal targets for studies of eruption dynamics; they erupt frequently, they have a relatively uniform crustal structure and basaltic

composition, and the magmatic systems are shallow and can be imaged seismically at high resolution.

Calderas are an important and complex feature of many volcanoes. Most high-resolution field constraints on the internal structure of the ring faults forming calderas come from geological studies of partially eroded calderas and these have led to a long-standing debate about their orientation and configuration at depth (Newhall and Dzurisin, 1988; Geyer and Marti, 2014). Earthquake observations at several locations support the existence of outward dipping ring faults (Mori and McKee, 1987; Mori et al., 1996; Ekström, 1994), however these existing studies have limited spatial resolution and there are no detailed observations of the role of ring faults in eruptions at basaltic volcanoes.

Axial Seamount is the most prominent volcanic feature on the Juan de Fuca mid-ocean ridge and is formed by the intersection of the ridge with the Cobb-Eickelberg hotspot. The summit at 1500 m depth is characterized by a 9 km by 3 km shallow caldera (Fig. 1a), which connects to rifts on the south and north flanks that form segments of the Juan de Fuca ridge. The caldera is underlain by a 14 km x 3 km magma and mush body with complex structure that is up to a kilometer thick, extends beyond both the northern and southern limits of the caldera and is slightly offset to the east (Arnulf et al., 2015). Diking-eruptive events in the southeast caldera and south rift in 1998 and 2011 were documented with seafloor pressure sensors (Fox et al. 1999; Chadwick et al., 2012) and hydrophones (Dziak and Fox, 1999; Dziak et al., 2012). While dike migration was observed for the 1998 eruption (Dziak and Fox, 1999), earthquake depths could not be constrained for these eruptions. The expectation of future eruptions motivated the deployment in 2014 of a multidisciplinary real-time cabled observatory on Axial Seamount (Kelley et al., 2014).

The cabled seismic network at the summit of Axial Seamount (Fig. 1) spans the southern half of the caldera, where the two prior recorded eruptions occurred, and comprises seven seismometers, three of which are collocated with bottom pressure and tilt sensors (Nooner and Chadwick, this issue). Seismic data are available starting in November 2014, with time corrected data streaming from late January 2015. In the first year of operation nearly 200,000 local earthquakes were detected and they show a temporal distribution (Fig. 2) that is similar to prior seafloor eruptions (Tolstoy et al., 2006, Dziak et al., 2012). Earthquake rates increase to $\sim$2000 day^{-1} leading up to the April 24th 2015 eruption then decrease rapidly following the seismic crisis, reaching a background level of 20 day^{-1} within a month.

Leading up to the eruption the earthquakes are strongly correlated with tides displaying clear peaks at the daily lowest low tide with secondary peaks often visible at the higher low tides (Fig. 2). Rates of seismicity are about six times greater during the lowest tide than the highest tide (Fig. S2a). This pattern can be attributed to the faults unclamping when the ocean loading is a minimum (Wilcock, 2001). However, the triggering weakens substantially post-eruption (Fig S2b),

suggesting it occurs primarily when the site is critically stressed in the months or years leading up to an eruption (Tolstoy et al., 2002, Stroup et al., 2007).

In the 3 months prior to the eruption, ~62,000 earthquakes were relocated using double difference methods (Waldhauser and Ellsworth, 2000). Most are small with a median moment magnitude (Mw) of 0.1 and only 35 have $M_W \geq 2$ (Fig. S3). Earthquakes are concentrated beneath the east and west walls of the caldera (Fig 1) with about five times as many beneath the east wall. In cross section (Fig. 1c) the earthquakes define outward dipping fault zones extending from near the surface to ~2 km depth. These zones dip at 60-70° with the dip decreasing slightly at shallow depths. Many of the remaining epicenters are located near the southern and northern ends of caldera and in a diffuse band of shallow seismicity that extends across the caldera just south of 45°57'N at a location that coincides with the southern boundary of the 2015 eruption and a northward transition from a melt rich to crystal mush magma chamber when imaged in 2002 (Arnulf et al., 2015).

For 6 hours preceding the start of the eruption, coincident with high tide, bursts of 7-10 Hz tremor are observed (Fig. 3) across the network, but are not coherent enough to locate. Tremor is not observed in the weeks prior, nor following the eruption, and is thus inferred to indicate magma movement within the caldera prior to crustal rupture. At ~0420, as the tremor ends, the rate and magnitude of seismicity starts to increase. Over about two hours the earthquake rate reaches a saturation level of 500-600 $hour^{-1}$ and the median magnitude increases from 0.5 to nearly 2. At ~0530, tilt sensors start to detect slight deformation, with more rapid deformation ~0615 (Nooner and Chadwick, this issue). Bottom pressure signals, indicating the start of caldera, collapse were observed at ~0600-0630, with a significant increase in rate around ~0700 (Nooner and Chadwick, this issue). Seismic energy levels peak between 0600 and 0730 and then decrease progressively through the day (Fig. 3).

The cumulative distribution of hypocenters for the eruption is similar to that beforehand with earthquakes concentrated near the east and west wall. Of 31 earthquakes on April 24 with Mw>2.5, all but one occur on the eastern side where the locations show a clear temporal pattern. Prior to 0600 the seismicity on the east wall is north of 45° 57'N with most of it, including all earthquakes with $M_W \geq 2.0$ north of 45°58'N. Over about 1.5 hours from 0615 to 0745 the locus of seismicity migrates 2.5 km south to 45°56.5'N (Fig. 3b and Fig. S4) consistent with the injection of a dike. Up until 0700 the earthquakes align closely with the north-south strike of southernmost eruptive fissures (Chadwick et al., this volume) suggesting that the fissure might be opening. After 0700 they follow the strike of the east wall. Earthquakes for the remainder of the crisis occur beneath the whole east wall but are concentrated south of the eruption between 45°56.5'N and 45°57.5'N where they are presumably associated with deflation.

Starting at 0801 on April 24, the seismic network recorded ~38,000 impulsive events (Fig. S1b) consistent with sound sources on the seafloor that propagate

through the water column and are detected on the seismometers as a train of reverberations. These events are spatially closely associated with all the new lava flows (Fig. 1a). The first impulsive event was observed within the caldera at 0801 with events then commencing successively on the flows to the north.

Impulsive acoustic signals from the seafloor associated with lava flows have been reported from several locations (Caplan-Auerbach and Duennebier, 2001; Chadwick et al., 2008; Schlindwein and Riedel, 2010; Dziak et al, 2015; Tan et al., 2016). Explosive mechanisms advanced to explain such signals include the expansion of magmatic gases in Strombolian eruptions, the release of trapped steam, and the combustion of hydrogen formed by the dissociation of water (Tribble, 1991). Strombolian eruptions are widespread at mid-ocean ridges (Clague et al., 2009) and have been identified as the source of volcanic signals in the Arctic Ocean (Sohn et al., 2008) as well as NW Rota-1 volcano in the Mariana arc and West Mata volcano in the Tonga-Kermadec arc where the eruptions were visually observed (Chadwick et al., 2008; Dziak et al, 2015). The presence of pyroclastic ash deposits associated with the 2015 Axial eruption (Chadwick et al., this issue) coupled with the high CO_2 contents of some lavas from prior eruptions (Helo et al., 2011) are consistent with the occurrence of similar explosions at Axial. However, the lava flows are also covered with numerous pits, which are interpreted in terms of small steam explosions (Chadwick et al., this issue).

Whatever the mechanisms it is clear the explosive signals start soon after magma reaches the seafloor (Tan et al., 2016). The first detected explosion within the caldera occurred within an hour of the onset of rapid deflation and earlier explosions may have been missed in the noise of the seismic crisis. The onset times on the north rift suggest that the dike propagated at a speed of 0.55 m/s. This is similar to observations in Iceland (Brandsdottir and Einarsson, 1979) but faster than the speed of 0.23 m/s observed for the 1998 eruption of Axial Seamount and thus consistent with the rapid deflation observed for this eruption (Nooner and Chadwick, this issue). The summit network detected no earthquakes associated with dike propagation along the north rift, a result of a shadowing effect from the elongated magma chamber and high noise levels from nearby earthquakes. However, dike propagation is supported by observations on a single seismic station 20 km southeast of the caldera (Fig. S5). We infer that the dike started northwards around 0700 at the outset of rapid deflation, taking ~2 hours at 0.5 m/s to reach the site of the first explosion on the north rift at 0904. Explosions near the northern end of the dike continued until May 21 (Fig. S6) which coincides with the time the caldera started to reinflate (Nooner and Chadwick, this issue), lending further support to a mechanism that links the explosions to fresh lava reaching the seafloor and showing that the plumbing system of the caldera links to the north rift dike.

The fault structure in the caldera is consistent with analog models obtained from sandbox simulations of caldera collapse due to underpressure (Roche et al., 2000; Kennedy et al., 2004; Buchard and Walter 2010) which show that with sufficient subsidence an outward dipping ring fault forms first followed by a peripheral

inward-dipping ring fault. At Axial Seamount, the outward dipping normal fault zones were active both during inflation and syn-eruptive deflation and they intersect the caldera floor about 0.75 km from walls. We infer that the caldera walls are formed by inward dipping normal faults that either deformed aseismically during this volcanic cycle or were only active while the caldera formed. The analog models predict that the outward dipping faults nucleate near the outer margins of the magma chamber. The separation of the fault zones we observe is consistent with the 3-4 km width of magma chamber (Arnulf et al., 2014) but the magma chamber is offset about 0.5-1 km east of the caldera. We speculate that the magma chamber may have migrated slightly eastward with the Cobb-Eickelberg hotspot melting anomaly since the caldera formed a minimum of 31 kyr ago (Clague et al., 2013). Comparisons of natural calderas with analog models suggests that the formation of two sets of ring structures requires a ratio of caldera diameter to subsidence less than ~14 (Acocella, 2007). For Axial Seamount the maximum height of the walls (160 m) and short- and long-axis dimensions yield a ratio of 20 and 50, respectively. However, the caldera has likely undergone substantial magmatic infilling since its formation (Clague et al., 2013).

The caldera substantially modulates the eruption. The north rift intersects the north rim of the caldera near its center but within and just to the north of the caldera the eruptive fissures are displaced 2 km to the east (Chadwick et al., this issue). Although it sits on an extensional mid-ocean ridge, we infer that the geometry of the outward dipping ring faults places the center of caldera in compression during inflation (Fig. 4), inhibiting the formation of extensional fractures that would extend the north rift into the caldera. Instead the eruption follows a trend that is sub parallel to the east wall and coincident with the zone of weakness of the outward dipping ring fault. The southward migration of earthquakes and change in the north-south tilt signal at the caldera center (Nooner and Chadwick, this issue) are consistent with the propagation of a dike which stalls upon reaching the northern limit of 1998 and 2011 eruptions. We infer that at the same time, the dike also migrated to the north following the same trend before stepping westward into the north rift. The first explosions from lavas on the seafloor in the caldera were observed an hour after the caldera started deflating rapidly and we speculate that some caldera deflation due to dike propagation in the rift may have been necessary to relieve compressional stresses in the caldera before magma could reach the caldera floor. Geodetic data suggest that eruptions at Axial volcano are triggered by a critical level of magmatic pressure (Nooner and Chadwick, this issue), and we speculate that this may be the pressure necessary to force magma laterally away from the compressional environment of the caldera into an extensional rift.

References:

Acocella, V. (2007). Understanding caldera structure and development: An overview of analogue models compared to natural calderas. *Earth-Science Reviews*, *85*(3), 125-160.

Arnulf, A. F., A. J. Harding, G. M. Kent, S. M. Carbotte, J. P. Canales and M. R. Nedimovic (2014), Anatomy of an active submarine volcano, *Geology, 42*, 655-658.

Brandsdottir, B., and P. Einarsson (1979). Seismic activity associated with the September 1977 deflation of the Krafla central volcano in northeastern Iceland. *Journal of Volcanology and Geothermal Research*, *6*(3-4), 197-212.

Buchardt, S. and T. Walter (2010). Propagation, linkage, and interaction of caldera ring-faults: comparisons between analogue experiments and caldera collapse at Miyakejima, Japan, in 2000. Bull Vulcanol. 72, 297-308

Caplan-Auerbach, J., and F. Duennebier (2001), Seismic and acoustic signals detected at Lo'ihi Seamount by the Hawai'i Undersea Geo-Observatory, Geochem. Geophys. Geosyst., 2, 1024, doi:10.1029/2000GC000113.

Chadwick, W. W.Jr., K. V. Cashman, R. W. Embley, H. Matsumoto, R. P. Dziak, C. E. J. de Ronde, T. K. Lau,N. D. Deardorff, and S. G. Merle (2008), Direct video and hydrophone observations of submarine explosive eruptions at NW Rota-1 volcano, Mariana arc, J. Geophys. Res., 113, B08S10, doi:10.1029/2007JB005215.

Chadwick, W. W., Jr., S. L. Nooner (2012), D. A. Butterfield, and M. D. Lilley, Seafloor deformation and forecasts of the April 2011 eruption at Axial Seamount, *Nat. Geosci., 5*, 474-477.

Clague, D. A., Paduan, J. B., & Davis, A. S. (2009). Widespread strombolian eruptions of mid-ocean ridge basalt. *J. Volcanol. Geotherm. Res.*, *180*(2), 171-188.

Clague, D. A. et al. (2013), Geologic history of the summit of Axial Seamount, Juan de Fuca Ridge, Geochem. Geophys. Geosyst.,14, 4403–4443, doi:10.1002/ggge.20240.

Crisp, J. A. (1984), Rates of magma emplacement and volcanic output, *J. Volcanol. Geotherm. Res.*, **20**,177–211.

Dziak, R. P., and Fox, C. G. (1999). The January 1998 earthquake swarm at Axial Volcano, Juan de Fuca Ridge: Hydroacoustic evidence of seafloor volcanic activity. Geophysical Research Letters, 26(23), 3429-3432.

Dziak, R. P., J. H. Haxel, D. R. Bohnenstiehl, W. W. Chadwick Jr., S. L. Nooner, M. J. Fowler, H. Matsumoto, and D. A. Butterfield (2012), Seismic precursors and magma ascent before the April 2011 eruption at Axial Seamount. *Nature Geoscience 5,* 478-482.

Ekström, G. (1994). Anomalous earthquakes on volcano ring-fault structures. *Earth and Planetary Science Letters*, *128*(3), 707-712.

Fox, C.G., W.W. Chadwick, R.W. Embley (2001). Direct observations of a submarine volcanic eruption from a sea-floor instrument caught in a lava flow, *Nature*, 412, 727-729, doi:10.1038/35089066

Geyer A., and J. Marti (2014), A short review of our current understanding of the development of ring faults during collapse caldera formation, *Frontiers Earth Sci., 2*(22), 1-13, doi:10.3389/feart.2014.00022.

Kelley, D. S., J. R. Delaney and S. K. Juniper (2014). Establishing a new era of submarine volcanic observatories: Cabling Axial Seamount and the Endeavour Segment of the Juan de Fuca Ridge, Mar. Geology, 352, 426-450.

Kennedy, B., J. Stix, J. W. Vallance, Y. Lavallee, and M.-A. Longpre (2004), Controls on caldera structure: results fron analogue sandbox modeling. Geol Soc. Am. Bull., 116, 515-524

Newhall, C. G. and D. Dzurisin, (1988) Historical unrest at large calderas of the world, *U.S. Geological Survey Bulletin, 1855*, 1108 pp.

Mori, J., and McKee, C. (1987). Outward-dipping ring-fault structure at Rabaul caldera as shown by earthquake locations. *Science*, *235*(4785), 193-195.

Mori, J., R. A. White, D. H. Harlow, P. Okubo, J. A. Power, R. P. Hoblitt, E. P. Laguerta, A. Lanuza, and B. C. Bautista (1996), Volcanic earthquakes following the 1991 climatic eruption of Mount Pinatubo: Strong seismicity during a waning eruption, in *Fire and Mud: Eruptions and Lahars of Mount Pinatubo, Philippines*, edited by C. G. Newhall and R. S. Punongbayan, University of Washington Press, Seattle, p. 335-350.

Roche, O., T. H. Druitt, and Merle, O. (2000), Experimental study of caldera formation, *J. Geophys. Res., 105*, 395-416.

Schlindwein, V., and C. Riedel (2010), Location and source mechanism of sound signals at Gakkel ridge, Arctic Ocean: Submarine Strombolian activity in the 1999–2001 volcanic episode, Geochem. Geophys. Geosyst., 11, Q01002, doi:10.1029/2009GC002706.

Sohn, R. A., Willis, C., Humphris, S., Shank, T. M., Singh, H., Edmonds, H. N., et al (2008). Explosive volcanism on the ultraslow-spreading Gakkel ridge, Arctic Ocean. *Nature*, *453*, 1236-1238.

Stroup, D. F., D. R. Bohnenstiehl, M. Tolstoy, F. Waldhauser, and R. T. Weekly (2007), Pulse of the seafloor: Tidal triggering of microearthquakes at 9°50′N East Pacific Rise, Geophys. Res. Lett., 34, L15301, doi:10.1029/2007GL030088.

Tan, Y. J., M. Tolstoy, F. Waldhauser, W.S.D Wilcock (2016), Plate boundary unzipped: Dynamics of a seafloor spreading episode at the East Pacific Rise, Nature, in review.

Tolstoy, M., Vernon, F. L., Orcutt, J. A., & Wyatt, F. K. (2002). Breathing of the seafloor: Tidal correlations of seismicity at Axial volcano. *Geology*, *30*(6), 503-506.

Tolstoy, M., Cowen, J.P., Baker, E.T., Fornari, D.J., Rubin, K.H., Shank, T.M., Waldhauser, F., Bohnenstiehl, D.R., Forsyth, D.W., Holmes, R.C. and Love, B., 2006. A sea-floor spreading event captured by seismometers. *Science*, *314*(5807), pp.1920-1922.

Tribble, G. W. (1991). Underwater observations of active lava flows from Kilauea volcano, Hawaii. *Geology*, *19*(6), 633-636.

Waldhauser, F., and W. L. Ellsworth, A double-difference earthquake location algorithm: Method and application to the northern Hayward Fault, California, *Bull. Seismol. Soc. Am.*, **90**, 1353–1368, 2000.

Wilcock, W. S. D. (2009), Tidal triggering of earthquakes in the Northeast Pacific OceanGeophys. J. Int., 179 (2), 1055-1070 doi:10.1111/j.1365-246X.2009.04319.x

Zobin, V. M. (2012), Introduction to Volcanic Seismology, Elsevier, 482 pp.

Figures

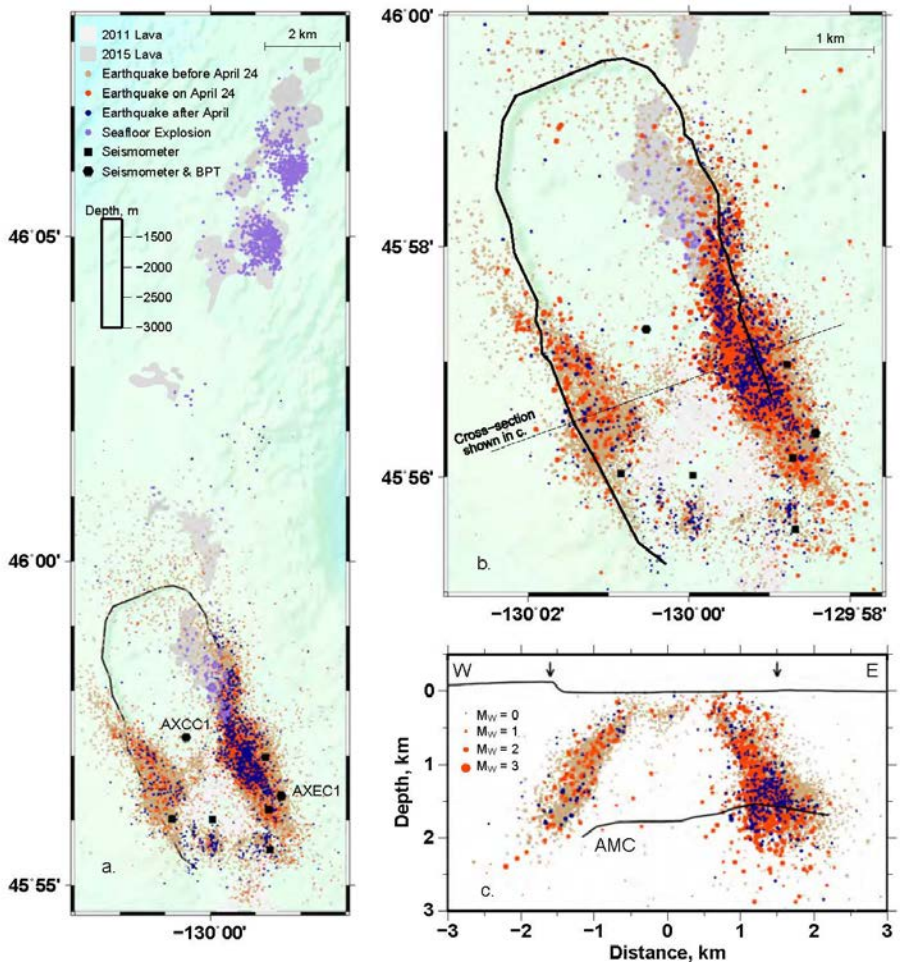

Figure 1. (a) Bathymetric map showing the seismic network and co-located bottom pressure and tilt (BPT) instruments, the distribution of epicenters color coded by time and seafloor explosions. (b) Epicenters and explosions in the caldera with symbol sizes scaled by magnitude. (c) Vertical cross section across the caldera showing the projected locations of earthquakes within 0.5 km of the profile. Also shows is the roof of the axial magma chamber (AMC) (Arnulf et al., 2014). Arrows show the margins of the caldera.

{NEED TO SHOW OUTLINE OF AMC IN MAP}

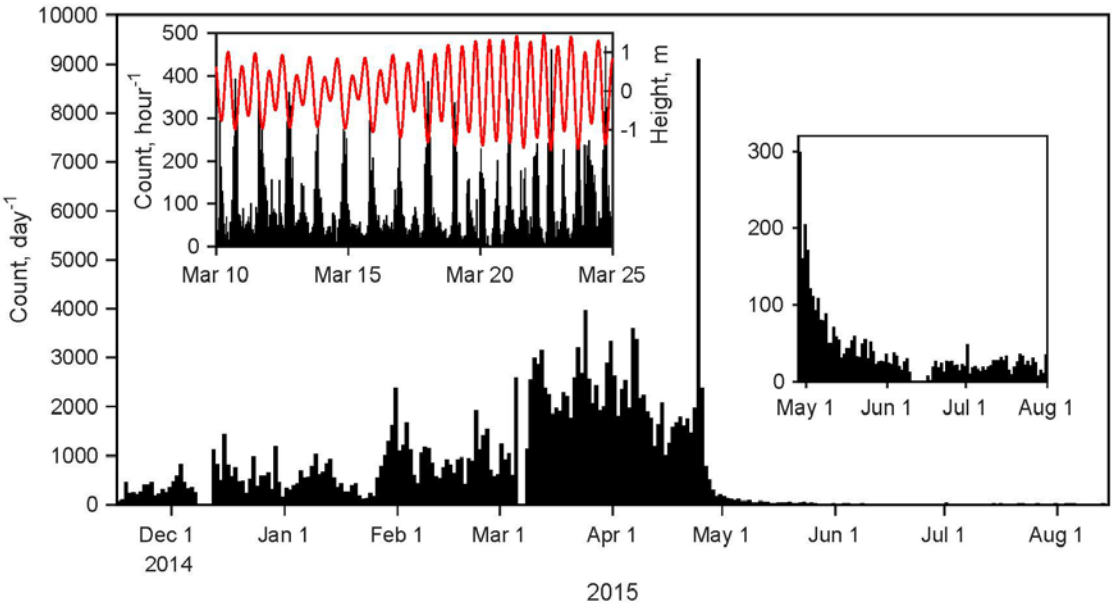

Figure 2. Histogram of earthquake detections for 9 months spanning the 2015 eruption. (Right inset) Magnification of the period after the eruption. (Left inset) Histogram of hourly detections for 15 days in March with ocean tides superimposed. Gaps in the histogram in December, March and June are intervals when data is unavailable.

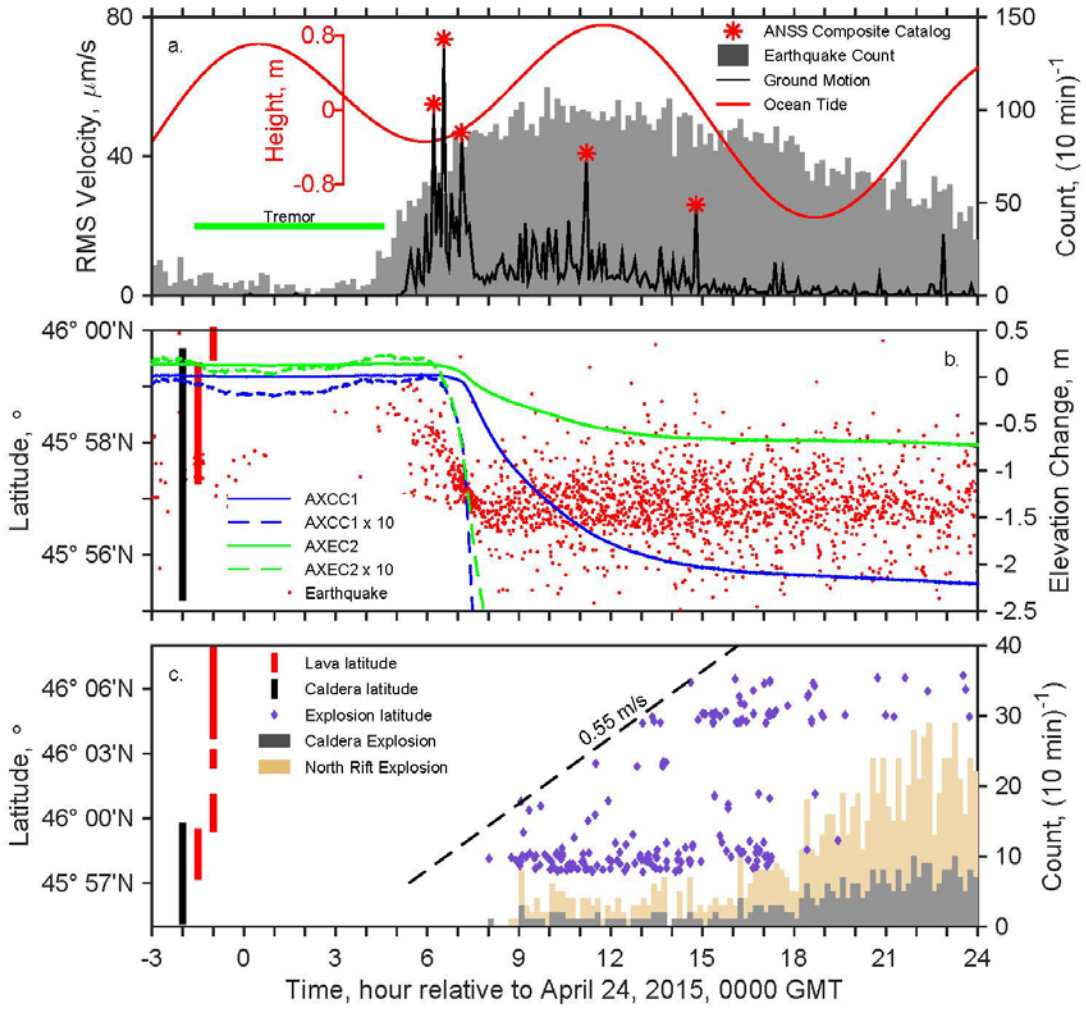

Figure 3. Chronology for the April 24, 2015 eruption. (a) Histogram of earthquake counts, RMS ground motion at station AXCC1 in the center of the caldera averaged over 5 minutes and ocean tides height. (b) Latitude of earthquakes beneath the east wall and the change in seafloor elevation recorded at stations AXCC1 and AXEC1 (from Nooner and Chadwick, this issue). (c) Histogram of explosions within the caldera and on the North rift and plot of latitudes for a subset of explosions.

{WILL SHOW MAGNITUDE OF EARTHQUAKES AND NEED TO GET COUNTS FOR CALDERA EXPLOSIONS FROM DEL}

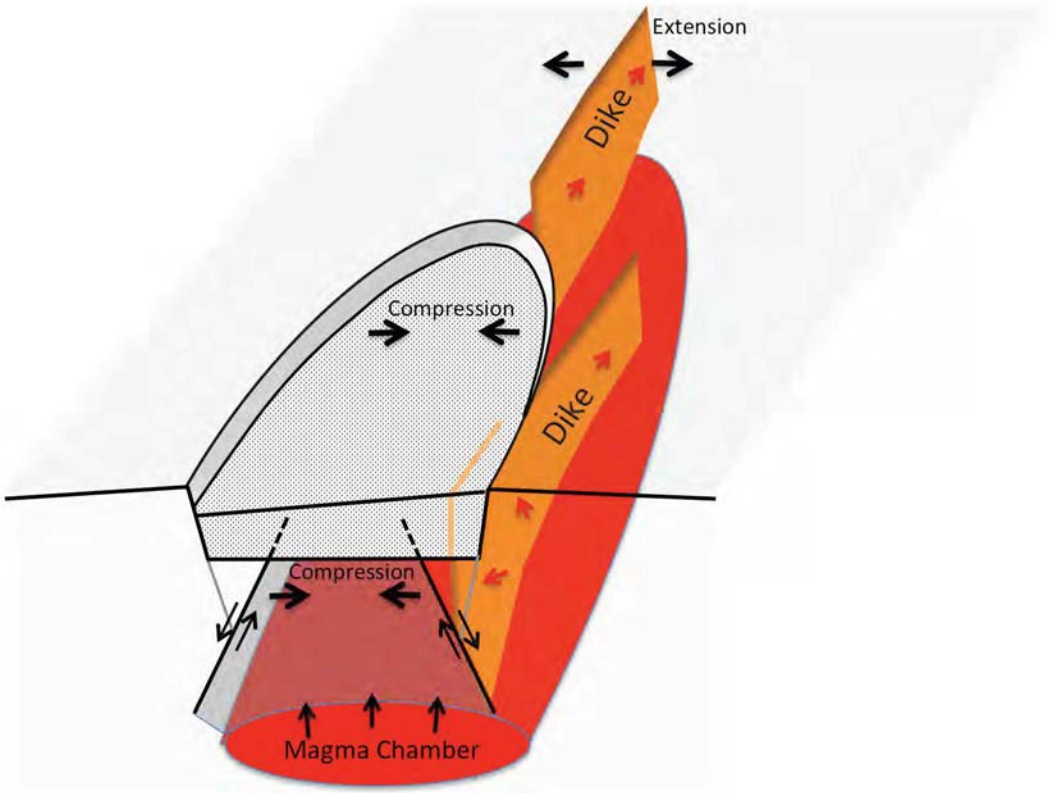

Figure 4. Cartoon illustrating the effect of the caldera ring fault on the eruption. The inflation of the magma chamber is accommodated by motion on the outward dipping ring faults that places the center of the caldera in compression and guides the eruption to east side of the caldera before the dike then steps westward into the extensional north rift.

{ADD LAVA FLOWS TO SEAFLOOR.}